arXiv:1702.03586v1 [cond-mat.str-el] 12 Feb 2017

Geometrically frustrated Cairo pentagonal lattice stripe with Ising and Heisenberg exchange interactions

F. C. Rodrigues, S. M. de Souza and Onofre Rojas[1]

Departamento de Física, Universidade Federal de Lavras, CP 3037, 37200-000, Lavras-MG, Brazil

Abstract

Motivated by the recent discoveries of some compounds such as the $Bi_2Fe_4O_9$ which crystallizes in an orthorhombic crystal structure with the Fe^{3+} ions, and iron-based oxyfluoride $Bi_4Fe_5O_{13}F$ compounds following the pattern of Cairo pentagonal structure, among some other compounds. We propose a model for one stripe of the Cairo pentagonal Ising-Heisenberg lattice, one of the edges of a pentagon is different, and this edge will be associated with a Heisenberg exchange interaction, while the Ising exchange interactions will associate the other edges. We study the phase transition at zero temperature, illustrating five phases: a ferromagnetic phase (FM), a dimer antiferromagnetic (DAF), a plaquette antiferromagnetic (PAF), a typical antiferromagnetic (AFM) and a peculiar frustrated phase (FRU) where two types of frustrated states with the same energy coexist. To obtain the partition function of this model, we use the transfer matrix approach and following the eight vertex model notation. Using this result we discuss the specific heat, internal energy and entropy as a function of the temperature, and we can observe some unexpected behavior in the low-temperature limit, such as anomalous double peak in specific heat due to the existence of three phase (FRU, PAF(AFM) and FM) transitions occurring in a close region to each other. Consequently, the low-lying energy thermal excitation generates this double anomalous peak, and we also discuss the internal energy at the low temperature limit, where this double peak curve occurs. Some properties of our result were compared with two dimensional Cairo pentagonal lattices, as well as orthogonal dimer plaquette Ising-Heisenberg chain.

Keywords: Pentagonal stripe; Ising-Heisenberg model; Geometric spin frustration

1. Introduction

In the past few years, the investigation in the Cairo pentagonal lattice has drawn much attention to researchers in condensed matter physics. The first

*email: ors@dfi.ufla.br

model proposed with the Cairo pentagonal Ising lattice structure was published in 2002 by Urumov[1], where the author studied as a purely theoretical physics problem, years later motivating a significant impact in pentagonal lattice investigation. More recently, the geometric frustration of Cairo pentagonal Ising model also was studied in more detail in reference [2]. By the year of 2009 Ressouche et al.[3] identified a compound $Bi_2Fe_4O_9$ which crystallizes in an orthorhombic structure with the Fe^{3+} ions, forming a first analogue with a magnetic Cairo pentagonal tessellation, where the Heisenberg exchange interaction describes the couplings with a good approximation. Furthermore, Ralko [4] studied the phase diagram of Cairo Pentagonal XXZ with spin-$1/2$ under a magnetic field, discussing the zero and finite temperature properties, using the stochastic series expansion and the cluster mean-field theory approach. Next, Rousochatzakis et al.[5] performed an extensive investigation both analytically and numerically, for the antiferromagnetic Heisenberg model on the Cairo pentagonal lattice. Following, Pchelkina and Streltsov[6] investigated the electronic structure and magnetic properties of compound $Bi_2Fe_4O_9$, forming a Cairo pentagonal lattice with strong geometric frustration. Besides, Abakumov et al.[7] reported a new crystal structure and magnetism of the iron-based oxyfluoride $Bi_4Fe_5O_{13}F$, and this compound also exhibits a Cairo pentagonal structure. Later, Isoda et al.[8] also studied the magnetic phase diagram under a magnetic field[8] as well as its magnetization process[9] of the spin-$1/2$ Heisenberg antiferromagnetic on the Cairo pentagonal lattice. More recently, a novel compound $Bi_2Fe_{4-x}Cr_xO_9$ ($x = 0.5, 1, 1.2$) has been synthesized using a soft chemistry technique followed by a solid-state reaction in Ar[10], which is a highly homogeneous mullite-type solid.

There are even more new compounds studied with the same structure, such the 2D crystals SnX_2 (X = S, Se, or Te)[11] which have been investigated using a first-principle calculation. Another investigation was carried out by Chainani and Sheshadri [12] for the Ising model with Cairo pentagonal pattern with a nearest-neighbor antiferromagnetic coupling. Finally, we can still comment on the new penta-graphene, recently discovered by Zhang et al.[13], although this compound is a non magnetic one, the penta-graphene pattern follows exactly the same Cairo pentagonal tessellation.

On the other hand, the Cairo pentagonal lattice Ising model[1, 2] is the dual of Shastry-Sutherland lattice Ising model[14]. Motivated by the Shastry-Sutherland lattice, Ivanov proposed a quasi one-dimensional Heisenberg model called as orthogonal dimer plaquette chain[15]. Certainly, the Cairo pentagonal chain can be viewed as a decorated orthogonal dimer chain[16, 17], where in our case the Ising spin would be considered as decorated spins. However, we cannot use the decoration transformation approach[21] naively to map the Cairo pentagonal chain into an orthogonal dimer chain, because we have quantum spins instead of classical spins (required condition to apply decoration transformation technique). Although there is a proposal for quantum spin decoration transformation approach[18], this transformation is exact only for isolated decorations, applying to a quantum spin lattice model would be just an approximate mapping.

The outline of this work is as follows. In sec. 2, we present the pentagonal Ising-Heisenberg chain, and we discuss the phase diagram at zero temperature. In sec. 3, we present the details to obtain the free energy calculation, and in sec. 4, we discuss some physical quantities obtained from free energy, such as the entropy, specific heat and internal energy. Finally, in sec. 5 we summarize our results and draw our conclusions.

2. Cairo pentagonal Ising-Heisenberg lattice stripe

Motivated by the comments given in the introduction we consider a stripe of the Cairo pentagonal lattice or decorated orthogonal dimer plaquette chain with Ising-Heisenberg coupling as schematically depicted in fig. 1.

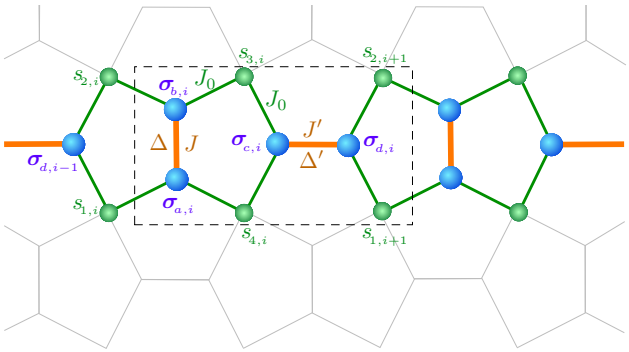

Figure 1: Schematic representation of the Cairo pentagonal Ising-Heisenberg lattice stripe, σ represents Heisenberg spins and s represents the Ising spins. The dashed rectangle represents an unit cell.

Let us define that the Hamiltonian for a Cairo pentagonal chain by

$$H = \sum_{i=1}^{N} \left(H_i^{ab} + H_{i,i+1}^{cd} \right), \tag{1}$$

where N is the number of cells and assuming periodic boundary condition. Thus, let us call as "elementary cell" ab-dimer and cd-dimer, which are described by H_i^{ab} and $H_{i,i+1}^{cd}$ respectively.

Therefore, each block Hamiltonian become

$$\begin{aligned} H_i^{ab} =& - J(\boldsymbol{\sigma}_{a,i}, \boldsymbol{\sigma}_{b,i})_{\Delta} - J_0(s_{1,i} + s_{4,i})\sigma_{a,i}^z + \\ & - J_0(s_{2,i} + s_{3,i})\sigma_{b,i}^z, \end{aligned} \tag{2}$$

$$\begin{aligned} H_{i,i+1}^{cd} =& - J'(\boldsymbol{\sigma}_{c,i}, \boldsymbol{\sigma}_{d,i})_{\Delta'} - J_0(s_{3,i} + s_{4,i})\sigma_{c,i}^z + \\ & - J_0(s_{1,i+1} + s_{2,i+1})\sigma_{d,i}^z, \end{aligned} \tag{3}$$

here $\sigma_{\gamma,i}^{\alpha}$ are the spin operators (with $\alpha = \{x, y, z\}$) at site i for particles $\gamma = \{a, b, c, d\}$, for detail see fig.1. The Ising spin exchange interaction parameter is

denoted by J_0, whereas J (J') represents the Heisenberg exchange interaction and Δ (Δ') means the anisotropic exchange interaction between Heisenberg spins for ab-dimer (cd-dimer) respectively. Whereas for ab-dimer $J(\boldsymbol{\sigma}_{a,i}, \boldsymbol{\sigma}_{b,i})_{\Delta}$ is defined by

$$J(\boldsymbol{\sigma}_{a,i}, \boldsymbol{\sigma}_{b,i})_{\Delta} \equiv J(\sigma^x_{a,i}\sigma^x_{b,i} + \sigma^y_{a,i}\sigma^y_{b,i}) + \Delta\sigma^z_{a,i}\sigma^z_{b,i}, \tag{4}$$

and for cd-dimer $J'(\boldsymbol{\sigma}_{a,i}, \boldsymbol{\sigma}_{b,i})_{\Delta'}$ is defined analogously to eq.(4).

2.1. Zero temperature phase diagram

To study the phase diagram at zero temperature, we need to describe the ground-state energy per unit cell. One elementary cell is composed by one dimer and bonded to 4 Ising spins. Each unit cell can be composed by two elementary cells: one ab-dimer and one cd-dimer, both dimers are bonded by 2 Ising spins. In fig.1 is illustrated one possible unit cell represented by a dashed rectangle.

The ground-state energy for each elementary cell could be described schematically using the fancy notations by

$$ab - \text{dimer} \longrightarrow |^{s_2}_{s_1}\rtimes^{s_3}_{s_4}\rangle \text{ and} \tag{5}$$
$$cd - \text{dimer} \longrightarrow |^{s_3}_{s_4}\ltimes^{s_5}_{s_6}\rangle, \tag{6}$$

where s_i correspond to the Ising spins, while the fancy symbols $\rtimes$ and $\ltimes$ denote four possible states as a function of $\{s_i\}$. Here, we use the spin subindex just for convenience, which cannot be confused with a more explicit spins notation in the Hamiltonian (2) and (3). Therefore, the eigenstates $|^{s_2}_{s_1}\rtimes^{s_3}_{s_4}\rangle$ of ab-dimers are conveniently expressed using four additional fancy notations, which are represented as follows

$$|\Join\rangle = |^{+}_{+}\rangle, \tag{7}$$
$$|\rtimes\rangle = \big(-\sin(\tfrac{\phi}{2})|^{+}_{-}\rangle + \cos(\tfrac{\phi}{2})|^{-}_{+}\rangle\big), \tag{8}$$
$$|\ltimes\rangle = \big(\cos(\tfrac{\phi}{2})|^{+}_{-}\rangle + \sin(\tfrac{\phi}{2})|^{-}_{+}\rangle\big), \tag{9}$$
$$|\barwedge\rangle = |^{-}_{-}\rangle, \tag{10}$$

where $\phi = \arctan\big(\frac{J}{J_0(s_1-s_2-s_3+s_4)}\big)$, with $-\pi \leqslant \phi \leqslant \pi$.

The first eigenstate $|^{+}_{+}\rangle$ of the ab-dimer (7) is denoted by $|\Join\rangle$, which is linked to spins $\{s_1, s_2, s_3, s_4\}$, thats why we use this fancy notation. Similarly, the eigenstate (10) is denoted by $|\barwedge\rangle$ which represents the states $|^{-}_{-}\rangle$ linked to the same set of spins $\{s_1, s_2, s_3, s_4\}$. Whereas, $|\rtimes\rangle$ denotes eq.(8) some kind of "anti-symmetric" state for $\phi > 0$, and $|\ltimes\rangle$ represents (9) some kind of "symmetric" state for $\phi > 0$, although for $\phi < 0$ this affirmation exchanges.

It is worth to mention that the states $|\Join\rangle$ and $|\barwedge\rangle$ are independent of Ising spins $\{s_1, s_2, s_3, s_4\}$, whereas states $|\rtimes\rangle$ and $|\ltimes\rangle$ depends of ϕ which subsequently depends of Ising spins $\{s_1, s_2, s_3, s_4\}$.

Whereas the corresponding energy eigenvalues for ab-dimer are given by

$$\begin{aligned}
\epsilon_1 &= -\tfrac{\Delta}{4} + \tfrac{J_0}{2}(s_1+s_4+s_2+s_3), && (11)\\
\epsilon_2 &= \tfrac{\Delta}{4} + \tfrac{1}{2}\sqrt{J_0^2(s_1+s_4-s_2-s_3)^2+J^2}, && (12)\\
\epsilon_3 &= \tfrac{\Delta}{4} - \tfrac{1}{2}\sqrt{J_0^2(s_1+s_4-s_2-s_3)^2+J^2}, && (13)\\
\epsilon_4 &= -\tfrac{\Delta}{4} - \tfrac{J_0}{2}(s_1+s_4+s_2+s_3). && (14)
\end{aligned}$$

Now using the eight-vertex model notation[1, 2, 19] and the fancy notations (7-10), we define six different states, explicitly including the Ising spins that connect the elementary cells by

$$\begin{aligned}
&|u_1\rangle = |{}^{+}_{+}\!\times^{+}_{+}\rangle, \quad |u_2\rangle = |{}^{-}_{+}\!\times^{+}_{-}\rangle, \quad |u_3\rangle = |{}^{-}_{+}\!\times^{-}_{+}\rangle,\\
&|u_4\rangle = |{}^{+}_{+}\!\times^{-}_{-}\rangle, \quad |u_5\rangle = |{}^{-}_{+}\!\times^{+}_{+}\rangle, \quad |u_7\rangle = |{}^{+}_{+}\!\times^{+}_{-}\rangle. \qquad (15)
\end{aligned}$$

The reason why we choose this notation could be more evident in the next section.

To obtain all 16 possible states, we can use in relation (15) the vertical and spin inversion symmetry, to recover 10 remaining states. Whereas each corresponding elementary cell ($|u_i\rangle$) energy is defined by ϵ_i, which have the following properties $\epsilon_2 = \epsilon_4$ and $\epsilon_5 = \epsilon_6 = \epsilon_7 = \epsilon_8$. Note that each $|u_i\rangle$ represents symbolically four states given by (7-10).

Analogously, we can obtain the corresponding states $|{}^{s_3}_{s_4}\!\times^{s_5}_{s_6}\rangle$, by the same relation to that (11-14), consequently the eigenvalues are expressed merely by substituting $J \to J'$, $\Delta \to \Delta'$ and $\{s_1, s_2, s_3, s_4\} \to \{s_6, s_4, s_3, s_5\}$.

Thus, the energy eigenvalues become

$$\begin{aligned}
\epsilon'_1 &= -\tfrac{\Delta'}{4} + \tfrac{J_0}{2}(s_6+s_5+s_4+s_3), && (16)\\
\epsilon'_2 &= \tfrac{\Delta'}{4} + \tfrac{1}{2}\sqrt{J_0^2(s_6+s_5-s_4-s_3)^2+J'^2}, && (17)\\
\epsilon'_3 &= \tfrac{\Delta'}{4} - \tfrac{1}{2}\sqrt{J_0^2(s_6+s_5-s_4-s_3)^2+J'^2}, && (18)\\
\epsilon'_4 &= -\tfrac{\Delta'}{4} - \tfrac{J_0}{2}(s_6+s_5+s_4+s_3). && (19)
\end{aligned}$$

Substituting $\phi \to \phi'$, the corresponding eigenstates read as follows

$$\begin{aligned}
|\!\uparrow\uparrow\rangle &= |++\rangle, && (20)\\
|\!\uparrow\downarrow\rangle &= -\sin(\tfrac{\phi'}{2})|+-\rangle + \cos(\tfrac{\phi'}{2})|-+\rangle, && (21)\\
|\!\downarrow\uparrow\rangle &= \cos(\tfrac{\phi'}{2})|+-\rangle + \sin(\tfrac{\phi'}{2})|-+\rangle, && (22)\\
|\!\downarrow\downarrow\rangle &= |--\rangle, && (23)
\end{aligned}$$

where $\phi' = \arctan\big(\frac{J'}{J_0(s_6+s_5-s_4-s_3)}\big)$, with $-\pi \leqslant \phi' \leqslant \pi$.

Similarly, the corresponding elementary states $|u_j\rangle \to |\bar{u}_j\rangle$ can be obtained by rotating in $\pi/2$ all 16 states. Then the first rotated state becomes $|\bar{u}_1\rangle = |{}^{+}_{+}\!\times^{+}_{+}\rangle$, thus all other states could be similarly obtained.

After defining each elementary cell, now we can construct the unit cell states by $|u_j\rangle \otimes |\bar{u}_k\rangle$. Once more, let us use the eight-vertex model notation[1, 2] to simplify the eigenstate of the unit cell,

$$|v_i\rangle = |{}^{s_2}_{s_1}\asymp^{s_3}_{s_4}\backsim^{s'_2}_{s'_1}\rangle. \tag{24}$$

Here becomes useful the fancy notation, because it relates the unit cell structure clearly. The unit cell state denoted by $|v_i\rangle$ are closely related with eight-vertex model notation for Ising spins $\{s_1, s_2, s'_2, s'_1\}$, here again we denote the Ising spins only for convenience by $s'_1 = s_6$ and $s'_2 = s_5$. Thus, the eq.(24) can be expressed as follows

$$\begin{aligned}
|v_1\rangle =& |{}^{+}_{+}\asymp^{s_3}_{s_4}\backsim^{+}_{+}\rangle, \quad |v_2\rangle = |{}^{-}_{+}\asymp^{s_3}_{s_4}\backsim^{+}_{-}\rangle, \\
|v_3\rangle =& |{}^{-}_{+}\asymp^{s_3}_{s_4}\backsim^{-}_{+}\rangle, \quad |v_4\rangle = |{}^{+}_{+}\asymp^{s_3}_{s_4}\backsim^{-}_{-}\rangle, \\
|v_5\rangle =& |{}^{-}_{+}\asymp^{s_3}_{s_4}\backsim^{+}_{+}\rangle, \quad |v_7\rangle = |{}^{+}_{+}\asymp^{s_3}_{s_4}\backsim^{+}_{-}\rangle.
\end{aligned} \tag{25}$$

It is worth mentioning that the unit cell convention allows expressing the eigenstates, this means that the edge of a unit cell must always connect the spins that share two neighboring unit cells. Thus, to satisfy the number of particles per unit cell, the leftmost and rightmost Ising spins must be shared by two unit cells, then each shared particle contributes with a half "particle" in the unit cell, as described by the fancy notations.

Certainly, each unit cell state $|v_i\rangle$ represents symbolically the $4 \times 4 \times 4 = 64$ possible states, the most relevant states are given by (25) and the remaining configurations can be obtained using horizontal symmetry and spin inversion symmetry.

Nevertheless, the rotational symmetry and the vertical symmetry are not allowed, because $|\asymp\backsim\rangle \neq |\backsim\asymp\rangle$, this means that the local chiral symmetry is broken in each unit cell, although the global chiral symmetry is preserved.

Using the previous result, we can study the phase diagram of the ground-state energy for the Cairo pentagonal chain per unit cell, thus we obtain

$$E_{_{FM}} = -2J_0 - \frac{\Delta}{2}, \tag{26}$$

$$E_{_{AFM}} = J_0 - \tfrac{1}{2}\sqrt{J^2 + 4J_0^2}, \tag{27}$$

$$E_{_{PAF}} = -J_0 - \tfrac{1}{2}\sqrt{J^2 + 4J_0^2}, \tag{28}$$

$$E_{_{DAF}} = 2J_0 - \frac{\Delta}{2}, \tag{29}$$

$$E_{_{FRU}} = \tfrac{1}{2}\Delta - \tfrac{1}{2}|J| - \tfrac{1}{2}\sqrt{J^2 + 4J_0^2}, \tag{30}$$

where we consider for simplicity $J' = J$ and $\Delta' = \Delta$.

Thus the system exhibits five states, whose ground-states can be expressed

by

$$|FM\rangle = \prod_{i=1}^{N} |^{+}_{+} \rtimes ^{+}_{+} \rangle \langle ^{+}_{+}\rangle_i \quad \text{or} \quad \prod_{i=1}^{N} |^{-}_{-} \asymp |^{-}_{-} \rangle \langle |^{-}_{-}\rangle_i, \tag{31}$$

$$|DAF\rangle = \prod_{i=1}^{N} |^{+}_{+} \asymp ^{+}_{+} \rangle \langle ^{+}_{+}\rangle_i, \quad \text{or} \quad \prod_{i=1}^{N} |^{-}_{-} \rtimes |^{-}_{-} \rangle \langle |^{-}_{-}\rangle_i, \tag{32}$$

$$|PAF\rangle = \prod_{i=1}^{N/2} |^{+}_{+} \rtimes ^{+}_{+} \rangle \bowtie ^{-}_{-} \asymp ^{-}_{-} \rangle \bowtie ^{+}_{+}\rangle_i, \tag{33}$$

$$|AFM\rangle = \prod_{i=1}^{N/2} |^{+}_{+} \asymp ^{+}_{+} \rangle \bowtie ^{-}_{-} \rtimes ^{-}_{-} \rangle \bowtie ^{+}_{+}\rangle_i. \tag{34}$$

The Cairo pentagonal Ising-Heisenberg chain can be described by the Hamiltonian (1), which exhibits five states (31-34): where we found a ferromagnetic (FM) phase; three types of antiferromagnetic phase, a dimer antiferromagnetic (DAF) phase, a plaquette antiferromagnetic (PAF) phase and one antiferromagnetic (AFM); Surely, the states (31-34) satisfy the spin inversion symmetry, all Ising and Heisenberg spins inversion leaves the system invariant.

The other state corresponding to the energy (30) is frustrated (FRU), represented symbolically by

$$|FRU\rangle = \begin{cases} \prod_{i=1}^{N} |^{\tau_{i-1}}_{\tau_{i-1}} \rtimes ^{-\tau_i}_{-\tau_i} \rangle \bowtie ^{\tau_i}_{\tau_i}\rangle_i, & \rightarrow \text{ Frustration type I,} \\ \prod_{i=1}^{N} |^{-\tau_i}_{\tau_i} \rtimes ^{-\tau_i}_{\tau_i} \rangle \bowtie ^{-\tau_{i+1}}_{\tau_{i+1}}\rangle_i, & \rightarrow \text{ Frustration type II,} \end{cases} \tag{35}$$

where τ_i ($\tau_{i,i+1}$) can take independently $\pm$ in each unit cell. We can recognize a frustrated state of type I is degenerate in 2^N states, since for each unit cell there are 2 degrees freedom (35). Similarly, for the frustration of type II becomes 2^N possible configurations (states) (35). Therefore, in total we have 2×2^N degenerate states. Notice that frustration type I and II cannot be mixed, because the linking spins of each unit cells are incompatible. Thus, we find a residual entropy $\mathcal{S} = k_B \ln(2 \times 2^N)/N = k_B \ln(2)$. It is worth remembering that the factor 2 that multiplies 2^N corresponds to two type of frustrations, but in thermodynamic limit this factor becomes irrelevant, this peculiar property is unusual for frustrated systems.

In fig.2a is illustrated the phase diagram Δ against J_0, for fixed $J = 1$, where we observe all five phases. The boundary between FM and PAF is given by $\Delta = -2J_0 + \sqrt{4J_0^2 + 1}$, analogously the interface between PAF and FRU is described by $\Delta = 1 - 2J_0$, similarly the boundary between DAF and AFM is limited by the curve $\Delta = 2J_0 + \sqrt{4J_0^2 + 1}$, whereas the boundary between AFM and FRU is described by $\Delta = 1 + 2J_0$. In fig.2b is depicted another phase diagram J versus Δ for a fixed parameter $J_0 = 1$. Illustrating once

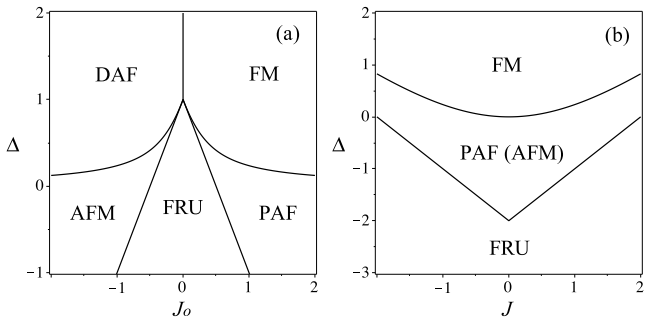

Figure 2: Ground-state phase diagram, where is illustrated a ferromagnetic phase (FM), a plaquette antiferromagnetic (PAF), a dimer antiferromagnetic (DAF) and a frustrated (FRU) phase. (a) In plane $J_0 - \Delta$, for fixed $J = 1$. (b) In plane $J - \Delta$, for fixed $J_0 = 1$.

again the previous phases displayed in fig.2a, whose boundary between FM and $PAF(AFM)$ is described by the curve $\Delta = -2 + \sqrt{4 + J^2}$, and similarly the interface between $PAF(AFM)$ and FRU is given by $\Delta = -2 + |J|$.

It is worth to mention that, the energy degeneracy in the boundary of DAF and FM per unit cell, each dimers (Heisenberg spins) contributes with 2^2 configurations ($\uparrow\uparrow, \downarrow\downarrow$) and 4 Ising spins with 2^4 configurations, thus the residual entropy is $\mathcal{S} = k_B \ln(2^{2N} \times 2^{4N})/N = 6k_B \ln(2)$. There is a point for $J_0 = 0$, $J = 1$ and $\Delta = 1$ where all phases coexist which is a highly frustrated phase, each dimers (Heisenberg spins) contributes with the triplet state ($\uparrow\uparrow, \downarrow\downarrow, \uparrow\downarrow$) and 4 Ising spins ($2^4$) whose residual entropy is $\mathcal{S} = k_B \ln(3^{2N} \times 2^{4N})/N = 2k_B \ln(12)$.

Using a similar reasoning in fig.2a, the curve surrounding the frustrated region, becomes a frustrated curve with a residual entropy $\mathcal{S} = k_B \ln(3)$, whereas the curve limiting the boundary between $FM(DAF)$ and $PAF(AFM)$ has a residual entropy $\mathcal{S} = k_B \ln(2)$.

At first glance, in fig.2a we can observe that for $\Delta > 0$ we could have a ferromagnetic coupling, so we should not expect a frustrated state in this region because the spins are aligned parallel to the z-axis. However, we observe a frustrated region for $\Delta > 0$, because the Heisenberg spins have projections on the xy components which contributes with $-|J|/2$ in eq.(30), thus generating a geometric frustration of quantum origin. Certainly, a quantum geometric frustration effect vanishes according $J \to 0$ becoming a classical geometric frustration.

Now let us compare the phase diagram of fig.2a with that two-dimensional Cairo pentagonal Ising model[2] which exhibits a ferrimagnetic state, for details see fig.4 of reference [2]. In the stripe of Cairo pentagonal lattice, there is no ferrimagnetic phase, in principle the DAF phase should be the responsible state to generate the ferrimagnetic phase in the two-dimensional lattice. It is easy to recognize the top and bottom particles will be sharing with neighboring unit cells, then, we will have a non-zero magnetization per unit cell, so generating a ferrimagnetic phase in two-dimensional lattice model. While the arise of AFM phase will not be allowed in two-dimensional lattice, because the sharing particle

spin will not be equivalent between unit cells, also a similar property forbids PAF in the two-dimensional lattice model. In a nutshell, the AFM and PAF phases only emerge in a one-dimensional pentagonal chain.

We can view the Cairo pentagonal chain as a decorated orthogonal dimer chain[16, 17], where in the Cairo pentagonal chain the Ising spin would be considered as a decorated spin. Therefore, we can compare the fig.2 with fig.3 of reference [16], and we observe that both figures are somewhat similar, particularly the phase boundaries. Although there is a difference between them, the orthogonal dimer chain does not exhibit a frustrated phase region[16], unless in the phase boundaries.

3. Thermodynamics of the model

The partition function of a Cairo pentagonal Ising-Heisenberg stripe can be obtained through the transfer matrix technique[19].

The Boltzmann factor for an ab-dimer elementary cell is given by

$$\mathsf{w}(s_{1,i}, s_{2,i}, s_{3,i}, s_{4.i}) = \mathrm{tr}_{ab}\left(\mathrm{e}^{-\beta H^{ab}_{i,i}}\right), \tag{36}$$

where $\beta = 1/k_B T$, with k_B being the Boltzmann's constant and T is the absolute temperature.

Whereas for a cd-dimer the Boltzmann factor is expressed by

$$\bar{\mathsf{w}}(s_{1,i+1}, s_{4,i}, s_{3,i}, s_{2.i+1}) = \mathrm{tr}_{cd}\left(\mathrm{e}^{-\beta H^{cd}_{i,i+1}}\right). \tag{37}$$

The best way to perform the trace is to diagonalize the Hamiltonian for ab-dimer and cd-dimer.

Using the standard 8-vertex model notation[19] as successfully used in two-dimensional spin lattice model[1, 2], we can express the Boltzmann factors for ab-dimer as follows

$$\omega_1 = \mathsf{w}(+,+,+,+) = z\left(x^4 + x^{-4}\right) + \frac{y^2 + y^{-2}}{z}, \tag{38}$$

$$\omega_2 = \mathsf{w}(+,-,+,-) = 2z + \frac{y^2 + y^{-2}}{z}, \tag{39}$$

$$\omega_3 = \mathsf{w}(+,+,-,-) = \omega_2, \tag{40}$$

$$\omega_4 = \mathsf{w}(+,-,-,+) = 2z + \frac{y_2^2 + y_2^{-2}}{z}, \tag{41}$$

$$\omega_5 = \mathsf{w}(+,+,+,-) = z\left(x^2 + x^{-2}\right) + \frac{y_1^2 + y_1^{-2}}{z}, \tag{42}$$

$$\omega_6 = \mathsf{w}(+,+,-,+) = \omega_5, \tag{43}$$

$$\omega_7 = \mathsf{w}(+,-,+,+) = \omega_5, \tag{44}$$

$$\omega_8 = \mathsf{w}(-,+,+,+) = \omega_5, \tag{45}$$

where $x = \mathrm{e}^{\beta J_0/4}$, $y = \mathrm{e}^{\beta J/4}$ and $z = \mathrm{e}^{\beta\Delta/4}$, we also define the following exponents $y_1 = \mathrm{e}^{\beta\sqrt{J^2+J_0^2}/4}$ and $y_2 = \mathrm{e}^{\beta\sqrt{J^2+4J_0^2}/4}$ just to simplify our notation.

Analogously, the Boltzmann factors for the *cd*-dimer are expressed in a similar way to the *ab*-dimer. Therefore, we have

$$\bar{\omega}_1 = \bar{\mathsf{w}}(+,+,+,+) = z'\left(x^4 + x^{-4}\right) + \frac{y'^2 + y'^{-2}}{z'}, \tag{46}$$

$$\bar{\omega}_2 = \bar{\mathsf{w}}(+,-,+,-) = 2z' + \frac{y'^2 + y'^{-2}}{z'}, \tag{47}$$

$$\bar{\omega}_4 = \bar{\mathsf{w}}(+,-,-,+) = 2z' + \frac{y_2'^{\,2} + y_2'^{\,-2}}{z'}, \tag{48}$$

$$\bar{\omega}_5 = \bar{\mathsf{w}}(+,+,+,-) = z'\left(x^2 + x^{-2}\right) + \frac{y_1'^{\,2} + y_1'^{\,-2}}{z'}, \tag{49}$$

where $y' = \mathrm{e}^{\beta J'/4}$ and $z' = \mathrm{e}^{\beta\Delta'/4}$, we define also the following exponents $y_1' = \mathrm{e}^{\beta\sqrt{J'^2+J_0^2}/4}$ and $y_2' = \mathrm{e}^{\beta\sqrt{J'^2+4J_0^2}/4}$. Moreover, we also have the following relations: $\bar{\omega}_2 = \bar{\omega}_3$ and $\bar{\omega}_5 = \bar{\omega}_6 = \bar{\omega}_7 = \bar{\omega}_8$.

To study the thermodynamics of the Cairo pentagonal Ising-Heisenberg chain, we observe that the Hamiltonian of each unit cell commutes between them. Consequently, the partition function could be written as the product of Boltzmann factors corresponding to the unit cells,

$$\mathcal{Z}_N = \mathrm{tr}\left(\prod_{i=1}^{N} \mathrm{e}^{-\beta(H_{i,i}^{ab} + H_{i,i+1}^{cd})}\right). \tag{50}$$

Therefore, the partition function (50) can be obtained using the transfer matrix approach, whose transfer matrix elements become

$$\mathsf{T}(s_1, s_2, s_1', s_2') = \sum_{s_3, s_4} \mathsf{w}(s_1, s_2, s_3, s_4)\bar{\mathsf{w}}(s_1', s_4, s_3, s_2'). \tag{51}$$

The matrices $\mathbf{w}$ and $\bar{\mathbf{w}}$ corresponding to *ab*-dimer and *cd*-dimer respectively, can be expressed explicitly by

$$\mathbf{w} = \begin{bmatrix} \omega_1 & \omega_5 & \omega_5 & \omega_3 \\ \omega_5 & \omega_4 & \omega_2 & \omega_5 \\ \omega_5 & \omega_2 & \omega_4 & \omega_5 \\ \omega_3 & \omega_5 & \omega_5 & \omega_1 \end{bmatrix}, \ \bar{\mathbf{w}} = \begin{bmatrix} \bar{\omega}_1 & \bar{\omega}_5 & \bar{\omega}_5 & \bar{\omega}_4 \\ \bar{\omega}_5 & \bar{\omega}_2 & \bar{\omega}_3 & \bar{\omega}_5 \\ \bar{\omega}_5 & \bar{\omega}_3 & \bar{\omega}_2 & \bar{\omega}_5 \\ \bar{\omega}_4 & \bar{\omega}_5 & \bar{\omega}_5 & \bar{\omega}_1 \end{bmatrix}. \tag{52}$$

It is worth mentioning that the matrices $\mathbf{w}$ and $\bar{\mathbf{w}}$ are fully symmetric matrices.

Thus, the transfer matrix $\mathbf{T}$ becomes

$$\mathbf{T} = \mathbf{w}\bar{\mathbf{w}} = \begin{bmatrix} \tau_1 & \tau_5 & \tau_5 & \tau_4 \\ \tau_7 & \tau_2 & \tau_3 & \tau_7 \\ \tau_7 & \tau_3 & \tau_2 & \tau_7 \\ \tau_4 & \tau_7 & \tau_7 & \tau_1 \end{bmatrix}, \tag{53}$$

where τ_i are the elements of transfer matrix, which are denoted following the eight-vertex model similar to that denoted in reference [1, 2]. Then τ_i are expressed by

$$\tau_1 = \omega_1\bar{\omega}_1 + \omega_3\bar{\omega}_4 + 2\omega_5\bar{\omega}_5, \tag{54}$$
$$\tau_2 = \omega_2\bar{\omega}_3 + \omega_4\bar{\omega}_2 + 2\omega_5\bar{\omega}_5, \tag{55}$$
$$\tau_3 = \omega_2\bar{\omega}_2 + \omega_4\bar{\omega}_3 + 2\omega_5\bar{\omega}_5, \tag{56}$$
$$\tau_4 = \omega_1\bar{\omega}_4 + \omega_3\bar{\omega}_1 + 2\omega_5\bar{\omega}_5, \tag{57}$$
$$\tau_5 = (\omega_2 + \omega_4)\,\bar{\omega}_5 + \omega_5\,(\bar{\omega}_1 + \bar{\omega}_4)\,, \tag{58}$$
$$\tau_7 = (\omega_1 + \omega_3)\,\bar{\omega}_5 + \omega_5\,(\bar{\omega}_2 + \bar{\omega}_3)\,, \tag{59}$$

and we can also verify that $\tau_3 = \tau_2$, $\tau_5 = \tau_6$ and $\tau_7 = \tau_8$.

Note that the transfer matrix $\mathbf{T}$ is a non-symmetric matrix, because in general $\tau_5 \neq \tau_7$, despite each $\mathbf{w}$ and $\bar{\mathbf{w}}$ are perfectly symmetric.

Thus, using the transfer matrix approach the partition function (50), can be written as

$$\mathcal{Z}_N = \mathrm{tr}\left[\left(\mathbf{w}\bar{\mathbf{w}}\right)^N\right] = \mathrm{tr}\left[\mathbf{T}^N\right]. \tag{60}$$

The eigenvalues of transfer matrix, can be obtained from $\det(\mathbf{T} - \lambda) = 0$, which results in,

$$\left(\lambda^2 - a_1\lambda + a_0\right)(\lambda - \tau_2 + \tau_3)\,(\lambda - \tau_1 + \tau_4) = 0, \tag{61}$$

where the coefficients of a quadratic equation are given by

$$a_1 = (\tau_1 + \tau_2 + \tau_3 + \tau_4)\,, \tag{62}$$
$$a_0 = (\tau_1 + \tau_4)\,(\tau_2 + \tau_3) - 4\tau_5\tau_7. \tag{63}$$

Consequently, the eigenvalues of the transfer matrix can be expressed as follows

$$\lambda_0 = \tau_2 - \tau_3 = 0, \tag{64}$$
$$\lambda_1 = \tau_1 - \tau_4, \tag{65}$$
$$\lambda_\pm = \tfrac{\tau_1+\tau_2+\tau_3+\tau_4}{2} \pm \tfrac{\sqrt{(\tau_1-\tau_2-\tau_3+\tau_4)^2+16\tau_5\tau_7}}{2}. \tag{66}$$

Although, the transfer matrix $\mathbf{T}$ is a non-symmetric one, we can observe that all eigenvalues are obviously real functions. Besides, one can readily identify, there is a largest eigenvalue positively defined λ_+, because all τ_i are positive real numbers following the relations (54-59).

In thermodynamic limit, the free energy per unit cell depends of the the largest eigenvalue of the transfer matrix, which is expressed by

$$f = -\frac{1}{\beta}\ln(\lambda_+)\,. \tag{67}$$

Using the free energy, we are able to obtain several thermodynamics quantities.

4. Physical quantities

In what follows we will discuss the entropy ($\mathcal{S} = -\frac{\partial f}{\partial T}$) property of the Cairo pentagonal chain, illustrating the regions where the model exhibits a frustrated sector as well as the different antiferromagnetic phases found in the previous section.

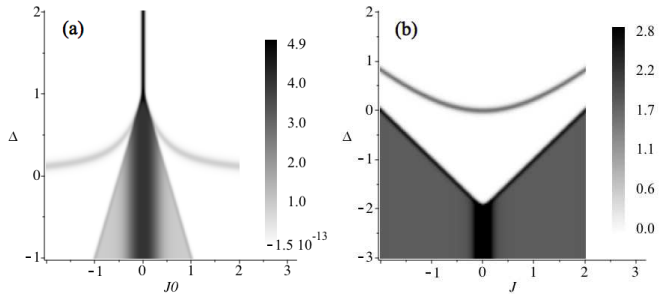

Figure 3: (a) Density plot of entropy as a function of J_0 and Δ, assuming fixed $J = 1$ and $T = 0.01$. (b) Density plot of entropy as a function of J against Δ for fixed $J_0 = 1.0$ and $T = 0.01$.

In fig.3a, we illustrate the density plot of the entropy as a function of J_0 and Δ for a fixed parameter $J = 1$ and in the low-temperature limit $T = 0.01$, darker regions correspond to higher entropies. Thus, we can readily verify the evidence of a frustrated region (FRU), with residual entropy $\mathcal{S} \to k_B \ln(2)$, and the boundary of this region is also a frustrated state with residual entropy $\mathcal{S} \to k_B \ln(3)$. Furthermore, there is a frustration curve in the interface of FM and DAF (PAF and AFM) both with residual entropy provided by $\mathcal{S} \to k_B \ln(2)$. The darkest region corresponds to $J_0 = 0$, $\Delta = 1$ and $J = 1$, which corresponds to a trivial frustrated phase composed by uncoupled *ab*-dimers and *cd*-dimers, so there are 4 Ising spins per unit cell and 2 triplet state (dimers) per unit cell, as discussed previously then the residual entropy leads to $\mathcal{S} \to 2k_B \ln(12) \approx 4.9698$.

Similarly, in fig.3b we illustrate the density plot of entropy in the plane J against Δ, in the low-temperature limit $T = 0.01$ and for fixed parameter $J_0 = 1$. Our results exhibit once again the presence of a frustrated region of the model (see fig.2). The darkest region corresponds to $J = 0$, thus, the Cairo pentagonal chain reduces to a pure Cairo pentagonal Ising chain with residual entropy $\mathcal{S} = 4k_B \ln(2) \approx 2.7726$, in this region we have an equivalent frustration to that found in reference [2].

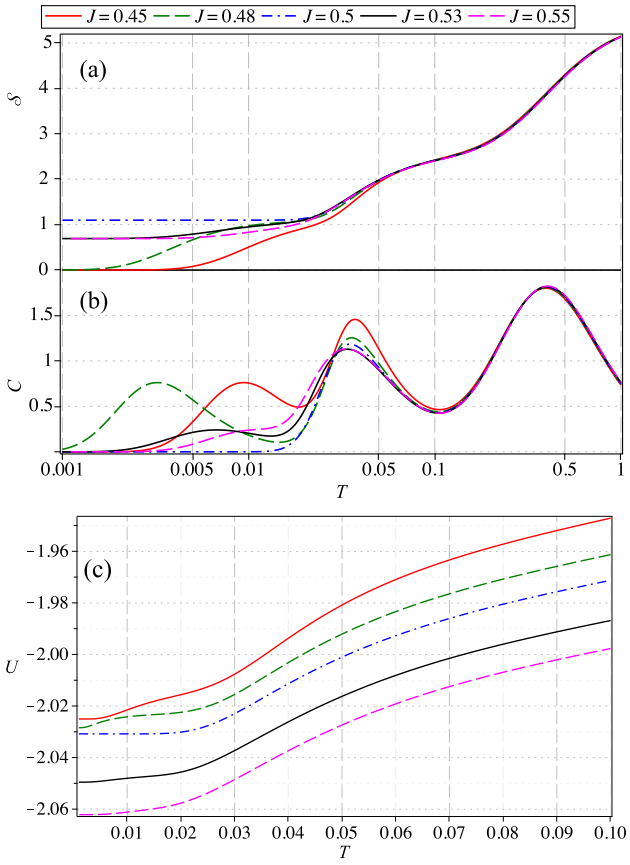

Figure 4: (a) Entropy as a function of the temperature, for fixed values of $J_0 = 1$ and $\Delta = -1.5$, for a range of values of $J = \{0.45, 0.48, 0.5, 0.53, 0.55\}$ in a logarithmic scale in temperature. (b) Specific heat as a function of temperature for a same set of parameters to the case (a). (c) Internal energy as a function of temperature for a same set of parameters to the case of (a), but on a linear scale for the temperature.

In fig. 4a, we display the entropy as a function of temperature assuming fixed parameter $J_0 = 1$ and $\Delta = -1.5$, for a range of $J = \{0.45, 0.48, 0.5, 0.53, 0.55\}$, using conveniently a logarithmic scale to show the low-temperature behavior, close to the phase transition illustrated in fig. 2b. Where we show the influence of zero temperature phase transition in the low-temperature limit, for $|J| \lesssim 0.5$ the system is highly influence by PAF(AFM) ground-state energy with residual entropy $\mathcal{S} \to 0$ when $T \to 0$, whereas frustrated energy contributes as low-lying excited energy, we can observe clearly residual entropy at $J = 0.5$ is given by $\mathcal{S} \to k_B \ln(3)$ when $T \to 0$. However for $J \gtrsim 0.5$, the system is dominated by a frustrated phase with residual entropy $\mathcal{S} \to k_B \ln(2)$ when $T \to 0$.

In fig.4b, we also discuss another interesting thermodynamic quantity called specific heat ($C = -T\partial^2 f/\partial T^2$). We illustrate for the same set of parameters

those considered in fig.4a and also on a logarithmic scale. Here we observe an anomalous double peak in the low-temperature region, which was influenced by the zero temperature phase transition between $PAF \leftrightarrow FRU$ and the low-lying energy responsible for FM state[22]. For $J = 0.45$ denoted by a solid (red) line, whose ground-state energy is non-degenerate and the first excited energy is macroscopically degenerate with a residual entropy $\mathcal{S} \to k_B \ln(2)$, when the temperature increases the contribution of the degenerate energy becomes more relevant than the contribution of the non-degenerate ground state, so the entropy curve is driven to behave like a frustrated system changing its concavity at $T \approx 0.003$, whereas for specific heat it manifests as a peak. Increasing the temperature slightly more we observe another change of concavity in entropy at $T \approx 0.03$, this is because there is another phase transition in the neighborhood (PAF between FM), the contribution of the excited low-lying energy level again drives the entropy (leading to a second peak in specific heat). A similar behavior was observed for a dashed (green) line assuming fixed $J = 0.48$ with a change of concavity in entropy at $T \approx 0.01$ and a second change of concavity occurs at $T \approx 0.03$, thus in specific heat we observe a double peak. Whereas for $J = 0.53$ (solid line), the change of the concavity in entropy at the lower temperature $T \approx 0.008$ is almost imperceptible, that is because the ground sate energy is macroscopically degenerate ($\mathcal{S} \to k_B \ln(2)$) and the lowest excited energy also becomes macroscopically degenerate ($\mathcal{S} \to k_B \ln(3)$), this is manifest as a small peak in the specific heat for $T \approx 0.008$. While the second peak in specific heat occurs at $T \approx 0.03$ basically by the same mechanism of low-lying excited energies. An analogous behavior we observe for $J = 0.55$ (magenta dashed line). Finally, for $J = 0.5$ (doted-dashed line) where the ground-state energy is macroscopically degenerate ($\mathcal{S} \to k_B \ln(3)$), and the low-lying excited energy (that originates from FM ground-state energy) generating just one change of concavity at around $T \approx 0.03$.

In fig. 4c, we plot the internal energy $U = f + T\mathcal{S}$, for the same set of parameters considered in fig. 4a, but here, we use a linear scale just to show the low-temperature internal energy behavior, to relate with specific heat anomalous peaks, since $C = \partial U/\partial T$ relates both quantities.

5. Conclusion

In this work we have proposed the Cairo pentagonal chain, motivated by recent discoveries of some compound such as the Fe^{3+} lattice in the $Bi_2Fe_4O_9$ and iron-based oxyfluoride $Bi_4Fe_5O_{13}F$ compounds with a Cairo pentagonal tiling. Therefore, we proposed one stripe of the Cairo pentagonal Ising-Heisenberg lattice. Subsequently, we have discussed the phase transition at zero temperature, illustrating five phases: one ferromagnetic (FM) phase, one dimer antiferromagnetic (DAF), one plaquette antiferromagnetic (PAF), one typical antiferromagnetic (AFM) phase and one peculiarly frustrated (FRU) phase, where coexist two type of frustrated states with same energy but without mixing these phases, this kind of frustration is very unusual. It is worth to mention also, for the case of two-dimensional pentagonal lattice the DAF phase, will be transformed into

a ferrimagnetic phase, due to the sharing spins between the unit cells. However, the AFM and PAF phase will be forbidden in a two-dimensional lattice, because the sharing spins between top and bottom unit cells will not be compatible.

To study the thermodynamics of this model we have used the transfer matrix approach and following the eight vertex model notation to find the partition function. Using this result, we have discussed the entropy and specific heat as a dependence of temperature. Accordingly, we observe an unusual behavior in the low-temperature limit, such as residual entropy and the anomalous double peak due the existence of three phases transition occurring in a very close region to each other and one of them is frustrated state. Thus, the thermal excitation of low-lying energy causes this anomalous double peak, and we also discussed the internal energy in the low-temperature limit, where occurred this double peak.

Acknowledgment

F. C. R. thanks Brazilian agency CAPES for full financial support. S. M. S. and O. R. thank Brazilian agencies, CNPq, FAPEMIG and CAPES for partial financial support. O. R. also thanks ICTP for partial financial support and the hospitality at ICTP.

References

[1] V. Urumov, J. Phys. A: Math. Gen. **35**, 7317 (2002).

[2] M. Rojas, O. Rojas and S. M. de Souza, Phys. Rev. E **86**, 051116 (2012).

[3] E. Ressouche, V. Simonet, B. Canals, M. Gospodinov, V. Skumryev, Phy. Rev. Lett. **103**, 267204 (2009).

[4] A. Ralko, Phys. Rev. B **84**, 184434 (2011).

[5] I. Rousochatzakis, A. M. Läuchli and R. Moessner, Phys. Rev. B **85**, 104415 (2012).

[6] Z.V. Pchelkina and S.V. Streltsov, Phys. Rev. B **88**, 054424 (2013).

[7] A. M. Abakumov, D. Batuk, A. A. Tsirlin, C. Prescher, L. Dubrovinsky, D. V. Sheptyakov, W. Schnelle, J. Hader- mann, and G. V. Tendeloo, Phys. Rev. B **87**, 024423 (2013).

[8] M. Isoda, H. Nakano, and T. Sakai, J. Phys. Soc. Jpn. **83**, 084710 (2014).

[9] H. Nakano, M. Isoda and T. Sakai, J. Phys. Soc. Jpn. **83**, 053702 (2014).

[10] M. G. Rozova, V. V. Grigoriev, I. A. Bobrikov, D. S. Filimonov, K. V. Zakharov, O. S. Volkova, A. N. Vasiliev, E. V. Antipov, A. A. Tsirlin, and A. M. Abakumov, Dalton Trans. **45**, 1192 (2016).

[11] Y. Ma, L. Kou, X. Li, Y. Dai, and T. Heine, NPG Asia Mater **8**, e264 (2016).

[12] A. Chainani, K. Sheshadri, arXiv:1412.6944

[13] S. Zhang, J. Zhou, Q. Wang, X. Chen, Y. Kawazoe, and P. Jena, Proc. Natl. Acad. Sci. USA **112**, 2372 (2015).

[14] B. S. Shastry and B. Sutherland, Physica B **108**, 1069 (1981).

[15] N. B. Ivanov and J. Richter, Phys. Lett. A **232**, 308 (1997).

[16] H. G. Paulinelli, S. M. de Souza, O. Rojas, J. Phys.: Condens. Matter **25**, 306003 (2013)

[17] T. Verkholyak, J. Strecka, Phys. Rev. B **88**, 134419 (2013); Acta Phys. Pol. A **126**, 22 (2014); arXiv:1607.08457

[18] F.F. Braz, F.C. Rodrigues, S.M. de Souza, O. Rojas, Annals of Physics **372**, 523 (2016).

[19] R.J. Baxter, Exactly Solved Models in Statistical Mechanics, (Academic Press, New York, 1982).

[20] O. Rojas and S. M. Souza J. Phys. A: Math. Theor. **44**, 245001 (2011).

[21] M. E. Fisher, Phys. Rev. **113**, 969 (1959); J. Strecka, Phys. Lett. A **374**, 3718 (2010); O. Rojas, J. S. Valverde and S. M. de Souza, Physica A **388**, 1419 (2009).

[22] K. Karlova, J. Strecka, T. Madaras, Physica B **488**, 49 (2016).